# Discrete breathers in square lattices from delocalized nonlinear vibrational modes

E. K. Naumov,[1,2,*] Yu. V. Bebikhov,[3,†] E. G. Ekomasov,[4,‡] E. G. Soboleva,[5,§] and S. V. Dmitriev[1,2,6,‖]

[1]*Institute of Molecule and Crystal Physics, UFRC of Russian Academy of Sciences, Ufa 450075, Russia*
[2]*Institute for Metals Superplasticity Problems of Russian Academy of Sciences, Khalturin Street 39, Ufa 450001, Russia*
[3]*Polytechnic Institute (Branch) in Mirny, North-Eastern Federal University, Tikhonova Street 5/1, 678170 Mirny, Sakha Republic (Yakutia), Russia*
[4]*Ufa University of Science and Technology, Zaki Validi 32, Ufa 450076, Russia*
[5]*National Research Tomsk Polytechnic University, Tomsk 634050, Russia*
[6]*Institute of Mathematics with Computing Centre, UFRC of Russian Academy of Sciences, Ufa 450000, Russia*

(Received 5 February 2023; accepted 15 March 2023; published 30 March 2023)

Standing and moving discrete breathers (or equally, intrinsic localized modes) in a square $\beta$-Fermi-Pasta-Ulam-Tsingou lattice are obtained by applying localizing functions to the delocalized nonlinear vibrational modes (DNVMs) found earlier by Ryabov and Chechin. The initial conditions used in our study do not correspond to exact spatially localized solutions, but make it possible to obtain long-lived quasibreathers. The approach employed in this work can easily be used to search for quasibreathers in three-dimensional crystal lattices, for which DNVMs with frequencies outside the phonon spectrum are known.

DOI: 10.1103/PhysRevE.107.034214

## I. INTRODUCTION

Discrete nonlinear systems support spatially localized large-amplitude oscillatory modes called discrete breathers (DBs) or intrinsic localized modes (ILMs). First DBs were discovered in nonlinear chains [1–3] and then in higher dimensional lattices [4,5], as well as in crystal lattices [6].

In higher dimensional lattices, different types of DBs can exist, and the problem of finding and classifying them arises. Delocalized nonlinear vibrational modes (DNVMs) [7–9], which have frequencies outside the phonon spectrum, help to solve this problem [10,11]. DNVMs are exact solutions to the equations of motion of particles, which can be found considering only the symmetry of the lattice; originally they were called bushes of nonlinear normal modes [7–9]. In the limit of small amplitude, DNVMs are transformed into short-wavelength phonon modes. Since only the symmetry of the lattice is taken into account in the derivation of DNVMs, they are exact solutions regardless of the type of interparticle interactions and for any amplitude. DNVM can have $m$ components; then it has $m$ degrees of freedom and can be described by $m$ coupled dynamical equations.

DNVMs are derived from irreducible representations of crystallographic symmetry groups [7–9]. An introduction to this approach can be found in the appendices of Refs. [12,13].

To the best of our knowledge, all DBs reported so far can be obtained by applying localizing functions to DNVMs having frequencies outside the phonon spectrum. This fact suggests that the search for DBs should be preceded by an analysis of DNVMs in the lattice under consideration. This approach was implemented for a triangular lattice, for which all one-component and two-component DNVMs were analyzed in Ref. [12] and it was shown that three of them have frequencies above the phonon spectrum. Then, in Ref. [11], various DBs were obtained by applying localizing functions to these three DNVMs.

Applying localization functions to DNVM usually does not lead to an exact DB solution, but rather to a long-lived quasibreather [14].

Recently Ryabov and Chechin have constructed 16 one-component DNVMs for square lattice [13] using the group-theoretical approach developed in Refs. [7–9]. Only two of them have frequencies above the phonon spectrum [13], which means that they can be used for obtaining spatially localized vibrational modes by applying localizing functions, and this work is carried out in the present study.

It is important to present the motivation for searching for DNVMs and DBs in model lattices and in crystals.

DBs affect the macroscopic properties of crystals [6,15], scatter phonons and thereby reduce thermal conductivity [16], and can initiate the formation and migration of lattice defects [17–19].

DNVMs and DBs are related to each other. DNVMs were used to search for DBs in a scalar square lattice [20]. DNVMs found for a chain and for a two-dimensional (2D) triangular lattice were employed to construct one- and two-dimensional DBs in fcc metals [21–23]. Recall that $k$-dimensional DB in $n$-dimensional lattice ($k < n$) is delocalized in $k$ dimensions and localized in $n - k$ dimensions. DNVMs were considered to obtain DBs in triangular Fermi-Pasta-Ulam-Tsingou (FPUT) lattice [11], in triangular Morse lattice [24,25], and

*jjjjenia@mail.ru
†bebikhov.yura@mail.ru
‡ekomasoveg@gmail.com
§sobolevaeno@mail.ru
‖dmitriev.sergey.v@gmail.com

 

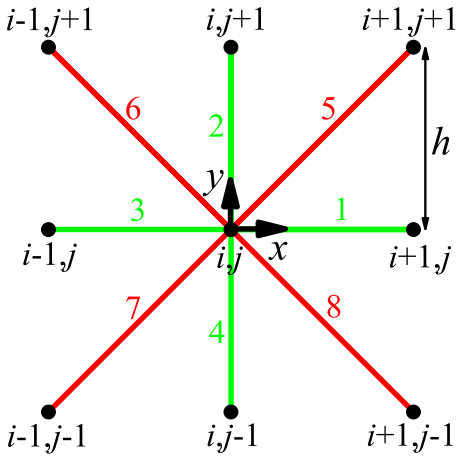


FIG. 1. Numbering of bonds and particles in the square lattice having step $h$. The nearest and next-nearest bonds are shown in green and red, respectively. The particles are numbered by the indices $i$ and $j$.

in bcc vanadium and niobium [10]. DNVMs of hexagonal lattice obtained in [26] were studied in graphene [27–30] and $h$-BN [31]. Modulational instability of DNVMs produces chaotic DBs [32–38]. The effect of chaotic DBs on macroscopic properties of triangular lattice was analyzed [39]. DNVMs help to check the accuracy of interatomic potentials used in molecular dynamics simulations [40].

It should also be discussed why the nonlinear dynamics of 2D lattices is of interest [41–44]. 2D lattices are used in many applications, for example, in the study of nonlinear excitations in mica [45–48] and model lattices [49–54]. It was shown that distortions of square lattice can open a gap in the phonon spectrum [55]. Moving periodic traveling waves were found in 2D lattices with saturable nonlinearity [56]. DBs with in-plane vibrations were identified in 2D FPUT lattices [57] and in topological ferromagnetic honeycomb lattices [58].

In the rest of the paper, the model is described in Sec. II. Then the phonon dispersion relation for the lattice is presented in Sec. III, one-component DNVMs are described in Sec. IV, and examples of analytical treatment of DNVMs are given in Sec. IV. In Sec. V, discrete breathers are obtained using localizing functions. The results are summarized and future problems are outlined in Sec. VI.

## II. FPUT SQUARE LATTICE

In Fig. 1, a two-dimensional square $\beta$-FPUT lattice with the lattice step $h$ is shown in the $xy$ plane. Each particle interacts with four nearest and four next-nearest neighbors. The basis vectors of the lattice are $\boldsymbol{e}_1 = (h, 0)$ and $\boldsymbol{e}_2 = (0, h)$. The lattice points have radius vectors

$$\boldsymbol{\xi}_{i,j} = i\boldsymbol{e}_1 + j\boldsymbol{e}_2, \tag{1}$$

where $i$ and $j$ are integers.

Particles of mass $m$ have two degrees of freedom, displacement vector components $(u_{i,j}, v_{i,j})$ from lattice positions. At time $t$ the particle $i, j$ has a radius vector $\boldsymbol{r}_{i,j}(t) = \boldsymbol{\xi}_{i,j} + (u_{i,j}(t), v_{i,j}(t))$.

Nearest ($n$) and next-nearest ($nn$) interactions are described by the $\beta$-FPUT potential

$$\varphi_{n,nn}(r) = \frac{k_{n,nn}}{2}(r - \alpha_{n,nn})^2 + \frac{\beta_{n,nn}}{4}(r - \alpha_{n,nn})^4, \tag{2}$$

where $r$ is the distance between the particles and $\alpha_n = h$ and $\alpha_{nn} = \sqrt{2}h$ are the equilibrium lengths of the nearest and next-nearest bonds, respectively; $k_n$ and $k_{nn}$ are the coefficients for the harmonic terms and the coefficients $\beta_n$ and $\beta_{nn}$ define the strength of anharmonicity for the nearest and next-nearest bonds, respectively.

Without loss of generality, we set $h = 1$ and $k_n = 1$ by choosing properly the units of distance and energy, respectively. For the harmonic stiffness of the next-nearest bonds, we also set $k_{nn} = 1$. The anharmonicity coefficients are set equal to $\beta_n = \beta_{nn} = 10$, and then nonlinearity comes into play at particle displacements of the order of $0.1h$. The particle mass is taken equal to $m = 1$, which can always be done by choosing the unit of time.

Let us define the following vectors connecting the particle $i, j$ with the nearest and next-nearest neighbors (see Fig. 1):

$$\begin{aligned}
&\boldsymbol{R}_{i,j,1} = \boldsymbol{r}_{i+1,j} - \boldsymbol{r}_{i,j}, \quad \boldsymbol{R}_{i,j,2} = \boldsymbol{r}_{i,j+1} - \boldsymbol{r}_{i,j},\\
&\boldsymbol{R}_{i,j,3} = \boldsymbol{r}_{i-1,j} - \boldsymbol{r}_{i,j}, \quad \boldsymbol{R}_{i,j,4} = \boldsymbol{r}_{i,j-1} - \boldsymbol{r}_{i,j},\\
&\boldsymbol{R}_{i,j,5} = \boldsymbol{r}_{i+1,j+1} - \boldsymbol{r}_{i,j}, \quad \boldsymbol{R}_{i,j,6} = \boldsymbol{r}_{i-1,j+1} - \boldsymbol{r}_{i,j},\\
&\boldsymbol{R}_{i,j,7} = \boldsymbol{r}_{i-1,j-1} - \boldsymbol{r}_{i,j}, \quad \boldsymbol{R}_{i,j,8} = \boldsymbol{r}_{i+1,j-1} - \boldsymbol{r}_{i,j}.
\end{aligned} \tag{3}$$

Computational cell includes $I$ particles along the $x$ axis and $J$ particles along the $y$ axis. The periodic boundary conditions are used: $\boldsymbol{r}_{i,j} = \boldsymbol{r}_{i+I,j} = \boldsymbol{r}_{i,j+J}$.

The Hamiltonian of the system is the sum of the kinetic ($K$) and potential energies of the nearest ($P_n$) and next-nearest ($P_{nn}$) bonds:

$$\begin{aligned}
H &= K + P_n + P_{nn}\\
&= \sum_{i=1}^{I}\sum_{j=1}^{J}\frac{m}{2}|\dot{\boldsymbol{r}}_{i,j}|^2\\
&\quad + \sum_{i=1}^{I}\sum_{j=1}^{J}\left(\sum_{k=1}^{2}\varphi_n(|\boldsymbol{R}_{i,j,k}|) + \sum_{l=5}^{6}\varphi_{nn}(|\boldsymbol{R}_{i,j,l}|)\right),
\end{aligned} \tag{4}$$

where $\dot{\boldsymbol{r}}_{i,j} = d\boldsymbol{r}_{i,j}/dt$.

The equations of motion obtained from Eq. (4) using the Hamilton's principle have the form

$$\begin{aligned}
m\ddot{u}_{i,j} &= \sum_{k=1}^{4} D_n R_{i,j,k,x} + \sum_{l=5}^{8} D_{nn} R_{i,j,l,x},\\
m\ddot{v}_{i,j} &= \sum_{k=1}^{4} D_n R_{i,j,k,y} + \sum_{l=5}^{8} D_{nn} R_{i,j,l,y},
\end{aligned} \tag{5}$$

where

$$D_n = \frac{\varphi_n'(|\boldsymbol{R}_{i,j,k}|)}{|\boldsymbol{R}_{i,j,k}|}, \quad D_{nn} = \frac{\varphi_{nn}'(|\boldsymbol{R}_{i,j,l}|)}{|\boldsymbol{R}_{i,j,l}|}. \tag{6}$$

The equations of motion Eq. (5) are integrated numerically using the Störmer method of order six [59] with the time step 0.002 time units.

The size of the simulation cell is taken equal to $I = J = 120$.

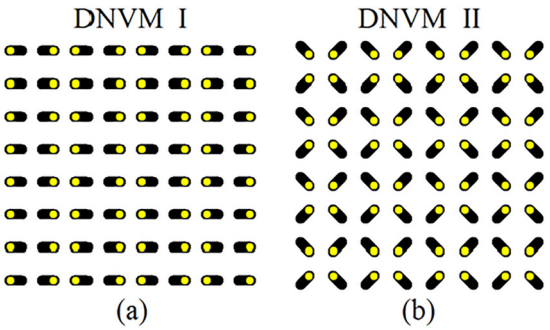


FIG. 2. Two one-component DNVMs in a square lattice having frequencies above the phonon spectrum. The DNVM amplitude is $A = 0.2$ in both cases. The particles are shown in yellow at the maximum deviation from the equilibrium positions, and the black lines show the trajectories of the oscillating particles. In the work [13], the DNVMs shown in panels (a) and (b) were numbered 1 and 16, but in this study they are numbered I and II, respectively.

## III. PHONON DISPERSION RELATION

Below the result of the work [13] is reproduced for the convenience of the reader.

For small deviations of particles from their lattice positions, $u_{ij} \ll h$ and $v_{ij} \ll h$, the equation of motion Eq. (5) can be linearized. Substituting into the linearized equations the standard form of the running wave solution, $u_{i,j} = U\exp[\mathrm{i}(qi + sj - \omega t)]$, $v_{i,j} = V\exp[\mathrm{i}(qi + sj - \omega t)]$, where i is an imaginary unit, one obtains the dispersion relation

$$\omega^2_{1,2}(q,s) = \frac{\gamma + \delta + \eta + \theta \pm \sqrt{(\gamma-\delta)^2 + (\eta-\theta)^2}}{2m}, \quad (7)$$

where

$$\gamma = 4k_n \sin^2\frac{q}{2}, \quad \delta = 4k_n \sin^2\frac{s}{2},$$
$$\eta = 4k_{nn} \sin^2\frac{q+s}{2}, \quad \theta = 4k_{nn} \sin^2\frac{q-s}{2}, \quad (8)$$

and $s$ and $q$ are the wave numbers.

For the points of the first Brillouin zone $(q,s) = (\pm\pi, 0)$ and $(0, \pm\pi)$ phonon frequencies are

$$\omega_1 = 2\sqrt{(k_n + k_{nn})/m}, \quad \omega_2 = 2\sqrt{k_{nn}/m}, \quad (9)$$

and for the points $(q,s) = (\pm\pi, \pm\pi)$

$$\omega_1 = \omega_2 = 2\sqrt{k_n/m}. \quad (10)$$

Frequency $\omega_1$ in Eq. (9) is the maximal phonon frequency. For chosen model parameters $k_n = k_{nn} = m = 1$ one has

$$\omega^{\max} = \sqrt{8}. \quad (11)$$

## IV. DNVMS WITH FREQUENCIES ABOVE THE PHONON SPECTRUM

As it was shown in Ref. [13], among 16 one-component DNVMs of square lattice only two have frequencies above the phonon spectrum for any amplitude; they are shown in Fig. 2. DNVMs I and II are single-degree-of-freedom dynamical systems. The frequency-amplitude dependence for the considered DNVMs is derived below within the cubic approximation.

### 1. DNVM I

Let $a(t)$ be the distance of the particle from the equilibrium position. The initial conditions for this dynamic variable are $a(0) = A$ and $\dot{a}(0) = 0$. Taking into account the symmetry of particle displacements in DNVM I, see Fig. 2(a), one obtains the following exact Hamiltonian:

$$H = \frac{m\dot{a}^2}{2} + \frac{1}{2}[\varphi_n(L_1 - h) + \varphi_{nn}(L_2 - \sqrt{2}h) + \varphi_{nn}(L_3 - \sqrt{2}h) + \varphi_n(L_4 - h) + \varphi_{nn}(L_5 - \sqrt{2}h) + \varphi_{nn}(L_6 - \sqrt{2}h)], \quad (12)$$

where

$$L_1 = h + 2a, \quad L_2 = \sqrt{(h+2a)^2 + h^2},$$
$$L_3 = \sqrt{(h-2a)^2 + h^2}, \quad L_4 = h - 2a, \quad (13)$$
$$L_5 = \sqrt{(h-2a)^2 + h^2}, \quad L_6 = \sqrt{(h+2a)^2 + h^2}.$$

Here $L_1$ and $L_4$ are distances between nearest neighbors, while $L_2$, $L_3$, $L_5$, and $L_6$ are distances between next-nearest neighbors.

The expansion of the potential energy in Eq. (12) in a Taylor series, up to fourth-order terms, leads to the simplified Hamiltonian

$$H = \frac{m\dot{a}^2}{2} + 2(k_n + k_{nn})a^2 + \left(4\beta_n + 2\beta_{nn} - \frac{3k_{nn}}{2h^2}\right)a^4. \quad (14)$$

The corresponding cubic equation of motion reads

$$m\ddot{a} = -4(k_n + k_{nn})a - \left(16\beta_n + 8\beta_{nn} - \frac{6k_{nn}}{h^2}\right)a^3. \quad (15)$$

Looking for the solution to Eq. (15) in the form $a(t) = A\sin(\omega t) + A_1\sin(3\omega t)$, where $A_1 \ll A$, one finds the frequency-amplitude relation in the form

$$\omega^2 \approx \frac{4}{m}(k_n + k_{nn}) + \frac{3}{4m}\left(16\beta_n + 8\beta_{nn} - \frac{6k_{nn}}{h^2}\right)A^2. \quad (16)$$

For the parameters used in our work, from Eq. (16) one has

$$\omega \approx \sqrt{8 + 175.5A^2}. \quad (17)$$

Indeed, frequency of DNVM I is above the phonon spectrum; see Eq. (11).

### 2. DNVM II

For DNVM II, taking into consideration the symmetry of particle displacements, see Fig. 2(b), one obtains the exact Hamiltonian

$$H = \frac{m\dot{a}^2}{2} + \frac{1}{2}[\varphi_n(L_1 - h) + \varphi_{nn}(L_2 - \sqrt{2}h) + \varphi_n(L_3 - h) + \varphi_{nn}(L_4 - \sqrt{2}h) + \varphi_n(L_5 - h) + \varphi_{nn}(L_6 - \sqrt{2}h) + \varphi_n(L_7 - h) + \varphi_{nn}(L_8 - \sqrt{2}h)], \quad (18)$$

where

$$L_1 = h + \frac{2a}{\sqrt{2}}, \quad L_2 = \sqrt{2h^2 + 4a^2},$$
$$L_3 = h - \frac{2a}{\sqrt{2}}, \quad L_4 = \sqrt{2}h - 2a,$$
$$L_5 = h - \frac{2a}{\sqrt{2}}, \quad L_6 = \sqrt{2}h - 2a,$$
$$L_7 = h - \frac{2a}{\sqrt{2}}, \quad L_8 = \sqrt{2h^2 + 4a^2}. \tag{19}$$

Here $L_1$, $L_3$, $L_5$, and $L_7$ are distances between nearest neighbors, and $L_2$, $L_4$, $L_6$, and $L_8$ are distances between next-nearest neighbors.

Expanding the potential energy in Eq. (18) in Taylor series and retaining up to fourth-order terms one obtains the simplified Hamiltonian

$$H = \frac{m\dot{a}^2}{2} + 4k_n a^2 + \left(6\beta_n + \frac{k_{nn}}{h^2}\right)a^4. \tag{20}$$

The corresponding cubic equation of motion is

$$m\ddot{a} = -8k_n a - 4\left(6\beta_n + \frac{k_{nn}}{h^2}\right)a^3. \tag{21}$$

Looking for the solution to Eq. (21) in the form $a(t) = A\sin(\omega t) + A_1\sin(3\omega t)$, where $A_1 \ll A$, one finds the frequency-amplitude relation:

$$\omega^2 \approx \frac{8k_n}{m} + \frac{3}{m}\left(6\beta_n + \frac{k_{nn}}{h^2}\right)A^2. \tag{22}$$

For the parameters used in our work, one finds from Eq. (22)

$$\omega \approx \sqrt{8 + 183A^2}. \tag{23}$$

DNVM II also has frequencies above the phonon spectrum; see Eq. (11).

In Fig. 3, the frequency response of DNVMs I and II is shown in red and blue, respectively. The numerically found frequencies are shown by circles and the theoretical estimates by lines. The analytical results obtained in the framework of the cubic approximation describe the numerical values quite well. The error increases with $A$, but for $A = 0.3$ it remains small: 1.26% for DNVM I and 0.96% for DNVM II.

## V. DISCRETE BREATHERS OBTAINED BY USING LOCALIZING FUNCTIONS

It is shown below that standing and moving DBs can be obtained by imposing a localizing function on DNVM I or DNVM II. Similarly, in the work [11] standing DBs for a triangular lattice were obtained.

We emphasize that the initial conditions used to excite DBs do not give exact spatially localized solutions, but make it possible to obtain long-lived quasibreathers [14]. Part of the energy initially transferred to the localized vibrational mode is radiated, and after the transition period, with the correct choice of the parameters of the localizing function, a quasibreather appears. The parameters of the localizing function are chosen in such a way that the energy emitted during stabilization of the quasibreather is minimal.

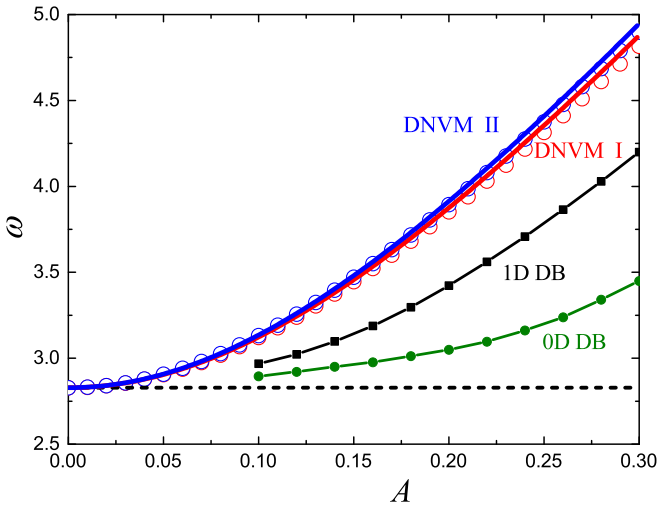


FIG. 3. Frequency response of DNVM I (red) and DNVM II (blue). The numerically found frequencies are shown by circles, and the lines show the analytical estimates Eqs. (17) and (23), respectively. The horizontal dashed line shows the upper edge of the phonon spectrum, Eq. (11). Black squares and green circles show the frequency-amplitude dependencies for the one-dimensional DB shown in Fig. 4(a) and zero-dimensional DB presented in Fig. 8(a), respectively.

In what follows, quasibreathers will be referred to as DBs.

### A. Stationary one-dimensional DBs

One-dimensional DB is localized along a line

$$p_1 x + p_2 y + p_3 = 0, \tag{24}$$

which means that the amplitudes of particle oscillations decay exponentially with distance from this line. This can be achieved by applying the localizing function

$$a_{ij} = \frac{A}{\cosh(\beta d_{ij})}, \tag{25}$$

where $a_{ij}$ is the magnitude of the initial displacement of particle having lattice position $\boldsymbol{\xi}_{i,j}$, $A$ is the DNVM amplitude, $\beta$ is the localization parameter, and $d_{ij}$ is the distance from the lattice point $i$, $j$ to the line Eq. (24), which can be calculated as follows:

$$d_{ij} = \frac{|p_1 x_{ij} + p_2 y_{ij} + p_3|}{\sqrt{p_1^2 + p_2^2}}. \tag{26}$$

It is assumed that $p_1$ and $p_2$ are not equal to zero simultaneously.

Initial velocities of all particles are equal to zero.

Figures 4 and 5 show examples of one-dimensional DBs based on DNVM I. The difference is that in Fig. 4 the DB localization line (shown in red) is parallel to the direction of particle oscillations, while in Fig. 5 it is perpendicular to this direction. In Fig. 5(a), the DB localization line passes through the row of particles, and in Fig. 5(b), it is in the middle between the nearest rows of particles. The parameters of the ansatz Eq. (25) are listed in the figure captions. Figure 5(c)

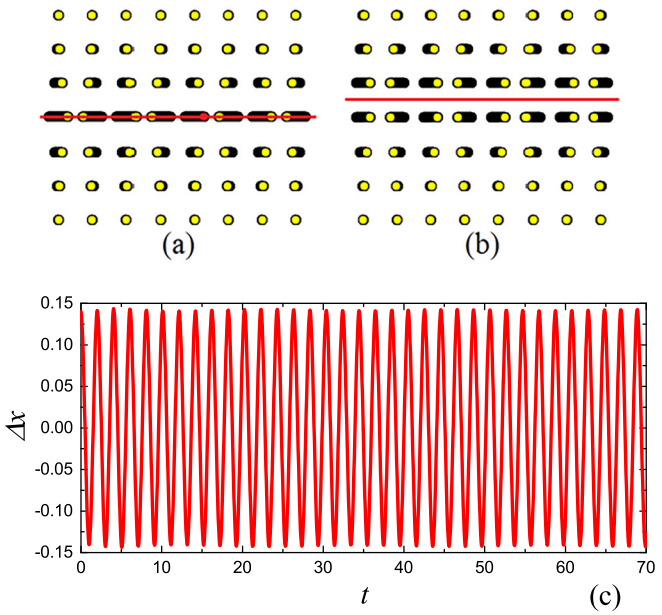


FIG. 4. Stationary one-dimensional DBs obtained by imposing localizing function Eq. (25) on DNVM I. The displacements are multiplied by a factor of 2. Parameters of the ansatz are (a) $p_1 = 0$, $p_2 = 1$, $p_3 = 0$, $A = 0.14$, $\beta = 1.48$; (b) $p_1 = 0$, $p_2 = 1$, $p_3 = h/2$, $A = 0.14$, $\beta = 1.45$. Lines of DB localization are shown in red. In panel (c), time evolution of the $x$ component of displacement of the particle colored red in panel (a) is presented.

shows the time evolution of the $x$ coordinates of particles colored red in Fig. 5(a). It can be seen that the particles perform periodic motion with constant amplitudes.

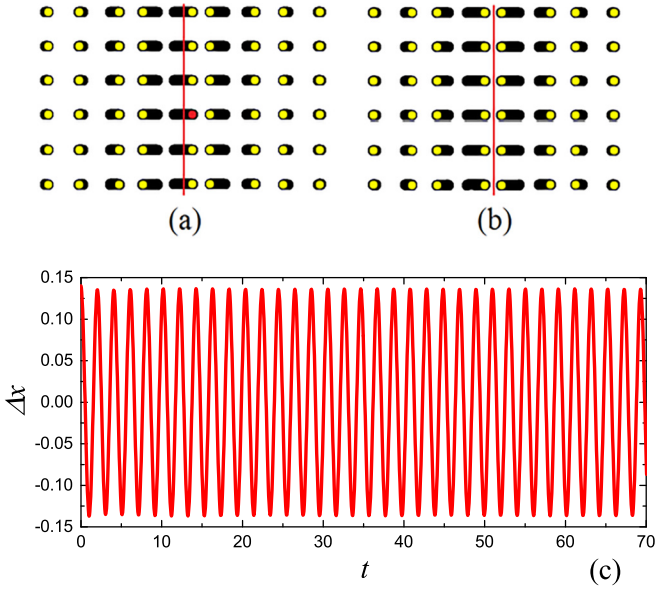


FIG. 5. Stationary one-dimensional DBs obtained by imposing localizing function Eq. (25) on DNVM I. The displacements are multiplied by a factor of 2. Parameters of the ansatz are (a) $p_1 = 1$, $p_2 = p_3 = 0$, $A = 0.14$, $\beta = 0.76$; (b) $p_1 = 1$, $p_2 = 0$, $p_3 = h/2$, $A = 0.14$, $\beta = 0.76$. Lines of DB localization are shown in red. In panel (c), time evolution of the $x$ component of displacement of the particle colored red in (a) is presented.

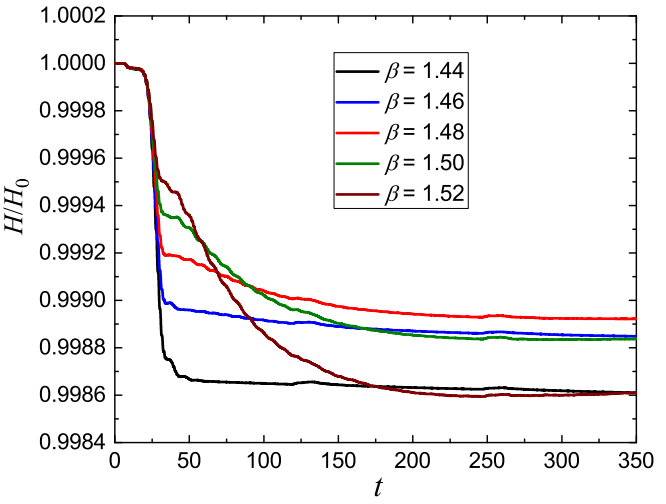


FIG. 6. The total energy of the system as a function of time, normalized to the initial energy obtained for the one-dimensional DB shown in Fig. 4(a), using different values of the localization parameter $\beta$. The other parameters of the ansatz Eqs. (25) and (26) are $p_1 = 0$, $p_2 = 1$, $p_3 = 0$, and $A = 0.14$. The total energy of the system decreases with time, since the energy emitted by the quasi-breather is absorbed at the boundaries of the computational cell. The smallest energy losses are observed at $\beta = 1.48$ and they increase when deviating from this value up or down.

As mentioned above, the localization parameter $\beta$ is chosen from the condition of minimizing the energy emitted during quasi-breather stabilization. This is illustrated in Fig. 6 for DB shown in Fig. 4(a) by plotting the time evolution of the total energy in the system normalized to the energy at $t = 0$. The total energy of the system decreases with time, since the energy emitted by the quasibreather is absorbed at the boundaries of the computational cell. After the emission of a portion of energy, the DB stabilizes and oscillates with a constant amplitude, practically radiating no energy. The smallest energy losses are observed at $\beta = 1.48$ and increase when deviating from this value up or down. Note that the total energy loss is only about 0.1% of the initial energy.

Figure 7 shows DBs based on DNVM II. In this case, one-dimensional DBs parallel to the close-packed lattice direction are impossible, but discrete breathers along the diagonal direction can be obtained. In Fig. 7(a), the DB localization line passes through particles oscillating along this line, and in Fig. 7(b), along particles oscillating in the normal direction. The parameters of the ansatz Eq. (25) are listed in the caption to the figure. In Fig. 7(c), the $x$ coordinates of particles colored in red and blue in in Fig. 7(b) are shown as functions of time by red and blue lines, respectively. The oscillation amplitudes are not constant, and a quasiperiodic energy exchange is observed between particles oscillating along and perpendicular to the DB line. However, DB remains localized for a long time.

### B. Stationary and moving zero-dimensional DBs

Zero-dimensional DB is localized at the point of intersection of two orthogonal lines,

$$p_1 x + p_2 y + p_3 = 0, \tag{27}$$
$$p_2 x - p_1 y + p_4 = 0, \tag{28}$$

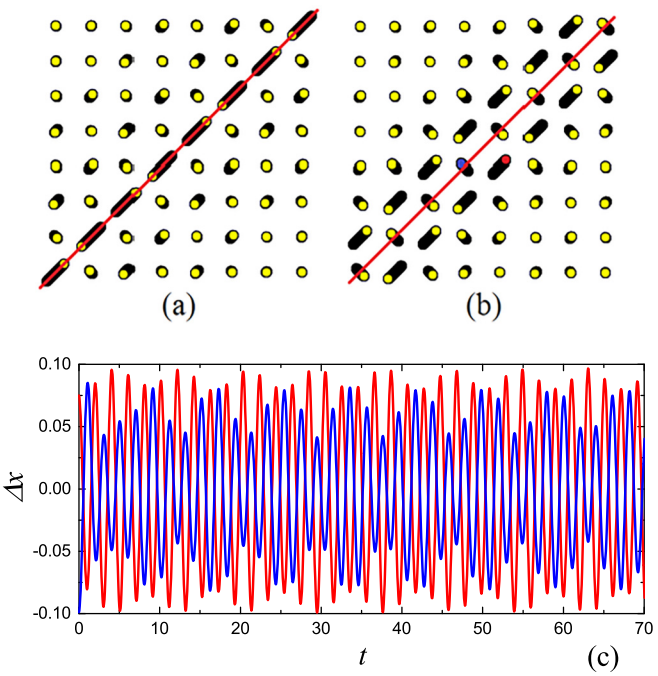


FIG. 7. Stationary one-dimensional DBs obtained by imposing localizing function Eq. (25) on DNVM II. The displacements are multiplied by a factor of 2. Parameters of the ansatz are (a) $p_1 = -1$, $p_2 = 1$, $p_3 = 0$, $A = 0.14$, $\beta = 1.1$; (b) $p_1 = -1$, $p_2 = 1$, $p_3 = h$, $A = 0.14$, $\beta = 1.1$. Lines of DB localization are shown in red. In panel (c), time evolution of the $x$ component of displacement of the particles colored red and blue in panel (b) are shown by the red and blue lines, respectively.

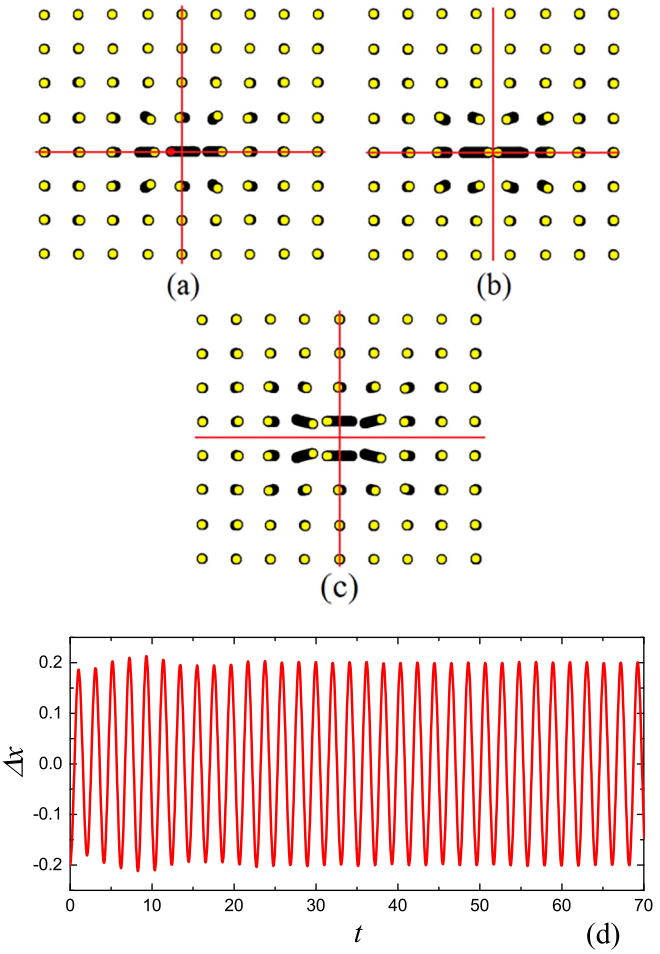


FIG. 8. Stationary zero-dimensional DBs obtained by imposing localizing function Eq. (30) on DNVM I. The displacements are multiplied by a factor of 2. Parameters of the ansatz are (a) $p_1 = 1$, $p_2 = 0$, $p_3 = 0$, $p_4 = 0$, $A = 0.2$, $\beta_1 = 1.05$, $\beta_2 = 1.5$; (b) $p_1 = 1$, $p_2 = 0$, $p_3 = h/2$, $p_4 = 0$, $A = 0.2$, $\beta_1 = 1.05$, $\beta_2 = 1.5$; (c) $p_1 = 1$, $p_2 = 0$, $p_3 = 0$, $p_4 = h/2$, $A = 0.25$, $\beta_1 = 1.05$, $\beta_2 = 1.5$. DBs are localized at the intersection of the red lines. In panel (d), time evolution of the $x$ component of displacement of the particle colored red in panel (a) is shown.

where $p_1$ and $p_2$ are not equal to zero simultaneously. The intersection point has coordinates

$$x_0 = \frac{-p_1 p_3 - p_2 p_4}{p_1^2 + p_2^2}, \quad y_0 = \frac{-p_2 p_3 + p_1 p_4}{p_1^2 + p_2^2}. \tag{29}$$

To construct zero-dimensional DBs, the localizing function is taken in the form

$$a_{ij} = \frac{A}{\cosh(\beta_1 d_{ij}) \cosh(\beta_2 f_{ij})}, \tag{30}$$

where $a_{ij}$ is the magnitude of the initial displacement of particle with the lattice position $\boldsymbol{\xi}_{i,j}$, $A$ is the DNVM amplitude, $\beta_1$ and $\beta_2$ are the localization parameters, $d_{ij}$ is the distance from the lattice point $i$, $j$ to the line Eq. (27), which is defined by Eq. (26), and $f_{ij}$ is the distance from the lattice point $i$, $j$ to the line Eq. (28), which is defined as

$$f_{ij} = \frac{|p_2 x_{ij} - p_1 y_{ij} + p_4|}{\sqrt{p_1^2 + p_2^2}}. \tag{31}$$

Examples of zero-dimensional DBs excited by imposing the localizing function Eq. (30) on DNVM I and DNVM II are shown in Figs. 8 and 9, respectively. DBs are localized at the intersection of two red lines. DBs with different position of the localization center are presented. In Fig. 8, the DB is localized (a) on a lattice cite, (b) shifted by the vector $(h/2, 0)$ from a lattice cite, and (c) shifted by the vector $(0, h/2)$ from a lattice cite. If the localization center is at the point $(h/2, h/2)$, DNVM I produces the DB shown in Fig. 9(a) as if DNVM II was used. In Fig. 9, the DB is localized (c) on a lattice cite, (a,d) shifted by the vector $(h/2, h/2)$ from the lattice cite, and (b) shifted by the vector $(3h/2, h/2)$ from the lattice cite. Figures 8(d) and 9(e) show time evolution of the $x$ component of displacement of the particle colored red in Figs. 8(a) and 9(a). It can be seen that stationary DBs with a constant oscillation amplitude are formed after a transition period of about 20 time units or 10 oscillation periods.

Stationary DBs are obtained when the center of localization is in a highly symmetrical lattice position. If the center of localization is displaced from the highly symmetrical position of the lattice, a moving DB can form. We tried different displacements of the center of localization for all obtained one-dimensional and zero-dimensional DBs, and only in one case did we obtain a moving DB. This is the case of the DB shown in Fig. 9(c), when the localization center is displaced from the lattice position along the line $y = x$. The DB moves

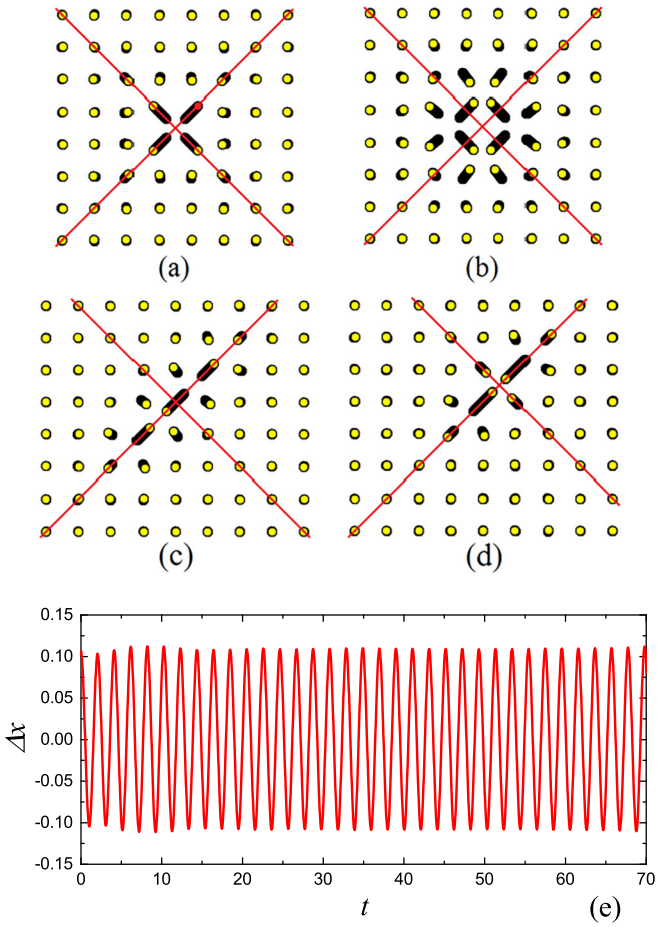


FIG. 9. Stationary zero-dimensional DBs obtained by imposing localizing function Eq. (30) on DNVM II. The displacements are multiplied by a factor of 2. Parameters of the ansatz are (a) $p_1 = -1, p_2 = 1, p_3 = 0, p_4 = h, A = 0.2, \beta_1 = \beta_2 = 1.11$; (b) $p_1 = -1, p_2 = 1, p_3 = h, p_4 = 0, A = 0.25, \beta_1 = \beta_2 = 1.12$. DBs are localized at the intersection of the red lines: (c) $p_1 = -1, p_2 = 1, p_3 = 0, p_4 = 0, A = 0.2, \beta_1 = 1.3, \beta_2 = 1.12$; (d) $p_1 = -1, p_2 = 1, p_3 = 0, p_4 = h, A = 0.2, \beta_1 = 1.8, \beta_2 = 0.6$. In panel (e), time evolution of the $x$ component of displacement of the particle colored red in panel (a) is shown.

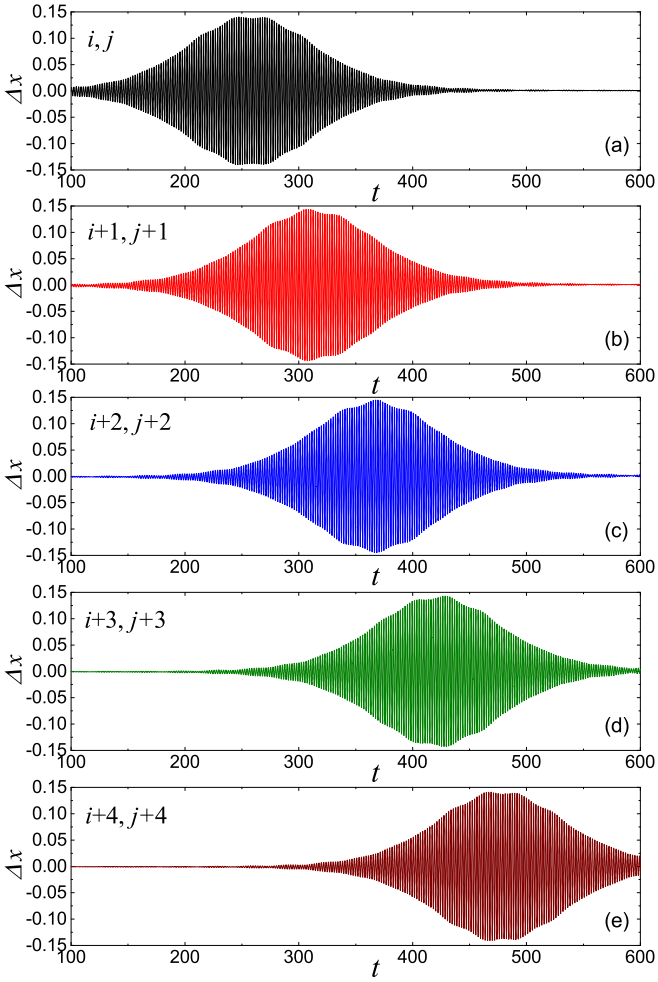


FIG. 10. Moving zero-dimensional DB obtained by imposing localizing function Eq. (30) on DNVM II. Shown is time evolution of the $x$ component of displacement of the particles (a) $i, j$, (b) $i+1, j+1$, (c) $i+2, j+2$, (d) $i+3, j+3$, and (e) $i+4, j+4$. Parameters of the ansatz are $p_1 = -1, p_2 = 1, p_3 = 0, p_4 = h/2, A = 0.2, \beta_1 = 1.3, \beta_2 = 1.12$.

along this line, as shown in Fig. 10, which presents the $x$ component of displacement of the particles (a) $i, j$, (b) $i+1, j+1$, (c) $i+2, j+2$, (d) $i+3, j+3$, and (e) $i+4, j+4$. It can be seen that the DB passes through these particles in turn. The DBs shown in Figs. 9(c) and 9(d) are the on-site and intersite versions of the moving DB, respectively.

It is interesting to see how the frequency of the constructed DBs is related to the frequency of the corresponding DNVM. In Fig. 3, the frequency-amplitude dependencies for one-dimensional and zero-dimensional DBs based on DNVM I are shown by black squares and green circles, respectively. The corresponding DBs are shown in Figs. 4(a) and 8(a), respectively. It can be seen that the DBs have frequencies lower than those of the DNVM. This is explained by the fact that in the DNVM all particles have an oscillation amplitude equal to $A$, while in the DB only particles of the core oscillate with an amplitude of $A$, while the remaining particles have a smaller oscillation amplitude. A decrease in the oscillation amplitude in a system with hard anharmonicity leads to a decrease in the oscillation frequency. This also explains why the softening of the zero-dimensional DB is stronger than that of the one-dimensional one.

## VI. CONCLUSIONS

In this study, zero- and one-dimensional discrete breathers in a $\beta$-FPUT square lattice are constructed by applying localizing functions on DNVMs I and II; see Fig. 2. These two DNVMs are among the 16 one-component DNVMs obtained by Ryabov and Chechin in Ref. [13], and their distinguishing feature is that they have frequencies above the phonon spectrum; see Sec. IV and Fig. 3.

One-dimensional DBs are localized along the line Eq. (24), while the amplitudes of particle oscillations decrease exponentially with distance from this line according to the ansatz Eq. (25). Zero-dimensional DBs are exponentially localized

at the intersection of two orthogonal lines Eqs. (27) and (28) according to the ansatz Eq. (30).

Stationary DBs are obtained by choosing localization lines along highly symmetric directions of the square lattice and localization points at highly symmetric points of the lattice. The parameters that determine the degree of spatial localization are chosen in such a way as to minimize the energy emitted by the DB during the transition period; see Fig. 6.

Four one-dimensional DBs based on DNVM I were obtained, two of them are parallel to the line $x = \text{const}$ (see Fig. 4), and the other two are parallel to the line $y = \text{const}$ (see Fig. 5). Two one-dimensional DBs based on DNVM II were obtained, parallel to the line $y = x$; see Fig. 7.

Three zero-dimensional DBs based on DNVM I were obtained, localized at the intersection of lines $x = \text{const}$ and $y = \text{const}$; see Fig. 8. Four zero-dimensional DBs based on DNVM II were obtained, localized at the intersection of lines $y = x$ and $y = -x$; see Fig. 9.

If the DB localization center is displaced from the highly symmetrical position of the lattice, a moving DB can form. We managed to set in motion only the DB shown in Fig. 9(c) by shifting the localization point from the lattice position along the line $y = x$; see Fig. 10.

Overall, the following findings were reported in this study. A method for constructing discrete breathers was applied to a square lattice by imposing localizing functions to DNVMs with frequencies above the phonon band. As a result, one-dimensional discrete breathers in a square lattice were described. Several zero-dimensional DBs were also built, including a moving DB.

Our work demonstrates that long-lived quasibreathers can be easily obtained by applying localizing functions to DNVMs that have frequencies outside the phonon spectrum. This method can be applied to lattices of higher dimensions. In future work, the frequency response of DNVMs in fcc, bcc, hcp, and other lattices will be analyzed for various interatomic potentials to find DNVMs that can be used to obtain quasibreathers.

The most important application of DNVMs, in our opinion, is the ability to use these high-amplitude exact dynamic solutions to test the accuracy of interatomic potentials used in molecular dynamics models by comparing with the results of first-principles simulations [40].

The data that support the findings of this study are available on request from the corresponding author, S.V.D.

## ACKNOWLEDGMENT

E.K.N. and S.V.D. acknowledge the support of the Russian Science Foundation, Grant No. 21-12-00229.

The authors declare that they have no conflict of interest.

[1] A. S. Dolgov, On localization of oscillations in nonlinear crystal structure, Sov. Phys. Solid State **28**, 907 (1986).

[2] A. J. Sievers and S. Takeno, Intrinsic Localized Modes in Anharmonic Crystals, Phys. Rev. Lett. **61**, 970 (1988).

[3] J. B. Page, Asymptotic solutions for localized vibrational modes in strongly anharmonic periodic systems, Phys. Rev. B **41**, 7835 (1990).

[4] S. Flach and C. R. Willis, Discrete breathers, Phys. Rep. **295**, 181 (1998).

[5] S. Flach and A. V. Gorbach, Discrete breathers—Advances in theory and applications, Phys. Rep. **467**, 1 (2008).

[6] S. V. Dmitriev, E. A. Korznikova, J. A. Baimova, and M. G. Velarde, Discrete breathers in crystals, Phys. Usp. **59**, 446 (2016).

[7] V. P. Sakhnenko and G. M. Chechin, Symmetrical selection rules in nonlinear dynamics of atomic systems, Phys. Dokl. **38**, 219 (1993).

[8] V. P. Sakhnenko and G. M. Chechin, Bushes of modes and normal modes for nonlinear dynamical systems with discrete symmetry, Phys. Dokl. **39**, 625 (1994).

[9] G. M. Chechin and V. P. Sakhnenko, Interactions between normal modes in nonlinear dynamical systems with discrete symmetry: Exact results, Phys. D (Amsterdam, Neth.) **117**, 43 (1998).

[10] K. A. Krylova, I. P. Lobzenko, A. S. Semenov, A. A. Kudreyko, and S. V. Dmitriev, Spherically localized discrete breathers in bcc metals V and Nb, Comput. Mater. Sci. **180**, 109695 (2020).

[11] R. I. Babicheva, A. S. Semenov, E. G. Soboleva, A. A. Kudreyko, K. Zhou, and S. V. Dmitriev, Discrete breathers in a triangular $\beta$-Fermi-Pasta-Ulam-Tsingou lattice, Phys. Rev. E **103**, 052202 (2021).

[12] D. S. Ryabov, G. M. Chechin, A. Upadhyaya, E. A. Korznikova, V. I. Dubinko, and S. V. Dmitriev, Delocalized nonlinear vibrational modes of triangular lattices, Nonlinear Dyn. **102**, 2793 (2020).

[13] D. S. Ryabov, G. M. Chechin, E. K. Naumov, Y. V. Bebikhov, E. A. Korznikova, and S. V. Dmitriev, One-component delocalized nonlinear vibrational modes of square lattices, Nonlinear Dyn. (2023), doi: 10.1007/s11071-023-08264-6.

[14] G. M. Chechin, G. S. Dzhelauhova, and E. A. Mehonoshina, Quasibreathers as a generalization of the concept of discrete breathers, Phys. Rev. E **74**, 036608 (2006).

[15] M. E. Manley, Impact of intrinsic localized modes of atomic motion on materials properties, Acta Mater. **58**, 2926 (2010).

[16] D. Xiong, J. Wang, Y. Zhang, and H. Zhao, Nonuniversal heat conduction of one-dimensional lattices, Phys. Rev. E **85**, 020102(R) (2012).

[17] J. Cuevas, J. F. R. Archilla, B. Sánchez-Rey, and F. R. Romero, Interaction of moving discrete breathers with vacancies, Phys. D (Amsterdam, Neth.) **216**, 115 (2006).

[18] T. Shimada, D. Shirasaki, and T. Kitamura, Stone-Wales transformations triggered by intrinsic localized modes in carbon nanotubes, Phys. Rev. B **81**, 035401 (2010).

[19] D. A. Terentyev, A. V. Dubinko, V. I. Dubinko, S. V. Dmitriev, E. E. Zhurkin, and M. V. Sorokin, Interaction of discrete breathers with primary lattice defects in bcc Fe, Modelling Simul. Mater. Sci. Eng. **23**, 085007 (2015).

[20] G. S. Bezuglova, G. M. Chechin, and P. P. Goncharov, Discrete breathers on symmetry-determined invariant manifolds for

scalar models on the plane square lattice, Phys. Rev. E **84**, 036606 (2011).
[21] O. V. Bachurina and A. A. Kudreyko, Two-dimensional discrete breathers in fcc metals, Comput. Mater. Sci. **182**, 109737 (2020).
[22] O. V. Bachurina, Plane and plane-radial discrete breathers in fcc metals, Modelling Simul. Mater. Sci. Eng. **27**, 055001 (2019).
[23] O. V. Bachurina, Linear discrete breather in fcc metals, Comput. Mater. Sci. **160**, 217 (2019).
[24] A. A. Kistanov, R. T. Murzaev, S. V. Dmitriev, V. I. Dubinko, and V. V. Khizhnyakov, Moving discrete breathers in a monoatomic two-dimensional crystal, JETP Lett. **99**, 353 (2014).
[25] E. A. Korznikova, S. Y. Fomin, E. G. Soboleva, and S. V. Dmitriev, Highly symmetric discrete breather in a two-dimensional Morse crystal, JETP Lett. **103**, 277 (2016).
[26] G. Chechin, D. Ryabov, and S. Shcherbinin, Large-amplitude in-plane atomic vibrations in strained graphene monolayer: Bushes of nonlinear normal modes, Lett. Mater. **10**, 523 (2020).
[27] E. Barani, I. P. Lobzenko, E. A. Korznikova, E. G. Soboleva, S. V. Dmitriev, K. Zhou, and A. M. Marjaneh, Transverse discrete breathers in unstrained graphene, Eur. Phys. J. B **90**, 38 (2017).
[28] E. A. Korznikova, S. A. Shcherbinin, D. S. Ryabov, G. M. Chechin, E. G. Ekomasov, E. Barani, K. Zhou, and S. V. Dmitriev, Delocalized nonlinear vibrational modes in graphene: Second harmonic generation and negative pressure, Phys. Status Solidi B **256**, 1800061 (2019).
[29] S. A. Shcherbinin, M. N. Semenova, A. S. Semenov, E. A. Korznikova, G. M. Chechin, and S. V. Dmitriev, Dynamics of a three-component delocalized nonlinear vibrational mode in graphene, Phys. Solid State **61**, 2139 (2019).
[30] D. U. Abdullina, M. N. Semenova, A. S. Semenov, E. A. Korznikova, and S. V. Dmitriev, Stability of delocalized nonlinear vibrational modes in graphene lattice, Eur. Phys. J. B **92**, 249 (2019).
[31] E. Barani, E. A. Korznikova, A. P. Chetverikov, K. Zhou, and S. V. Dmitriev, Gap discrete breathers in strained boron nitride, Phys. Lett. A **381**, 3553 (2017).
[32] R. Stearrett and L. Q. English, Experimental generation of intrinsic localized modes in a discrete electrical transmission line, J. Phys. D: Appl. Phys. **40**, 5394 (2007).
[33] B. Tang and K. Deng, Discrete breathers and modulational instability in a discrete $\phi^4$ nonlinear lattice with next-nearest-neighbor couplings, Nonlinear Dyn. **88**, 2417 (2017).
[34] E. A. Korznikova, D. V. Bachurin, S. Y. Fomin, A. P. Chetverikov, and S. V. Dmitriev, Instability of vibrational modes in hexagonal lattice, Eur. Phys. J. B **90**, 23 (2017).
[35] L. Kavitha, A. Mohamadou, E. Parasuraman, D. Gopi, N. Akila, and A. Prabhu, Modulational instability and nano-scale energy localization in ferromagnetic spin chain with higher order dispersive interactions, J. Magn. Magn. Mater. **404**, 91 (2016).
[36] L. Kavitha, E. Parasuraman, D. Gopi, A. Prabhu, and R. A. Vicencio, Nonlinear nano-scale localized breather modes in a discrete weak ferromagnetic spin lattice, J. Magn. Magn. Mater. **401**, 394 (2016).
[37] K. Ikeda, Y. Doi, B.-F. Feng, and T. Kawahara, Chaotic breathers of two types in a two-dimensional Morse lattice with an on-site harmonic potential, Phys. D (Amsterdam, Neth.) **225**, 184 (2007).
[38] E. A. Korznikova, A. Y. Morkina, M. Singh, A. M. Krivtsov, V. A. Kuzkin, V. A. Gani, Y. V. Bebikhov, and S. V. Dmitriev, Effect of discrete breathers on macroscopic properties of the Fermi-Pasta-Ulam chain, Eur. Phys. J. B **93**, 123 (2020).
[39] A. Upadhyaya, M. N. Semenova, A. A. Kudreyko, and S. V. Dmitriev, Chaotic discrete breathers and their effect on macroscopic properties of triangular lattice, Commun. Nonlinear Sci. Numer. Simul. **112**, 106541 (2022).
[40] S. A. Shcherbinin, K. A. Krylova, G. M. Chechin, E. G. Soboleva, and S. V. Dmitriev, Delocalized nonlinear vibrational modes in fcc metals, Commun. Nonlinear Sci. Numer. Simul. **104**, 106039 (2022).
[41] X. Yi, J. A. D. Wattis, H. Susanto, and L. J. Cummings, Discrete breathers in a two-dimensional spring-mass lattice, J. Phys. A: Math. Theor. **42**, 355207 (2009)
[42] I. A. Butt and J. A. D. Wattis, Discrete breathers in a two-dimensional hexagonal Fermi-Pasta-Ulam lattice, J. Phys. A: Math. Theor. **40**, 1239 (2007).
[43] I. A. Butt and J. A. D. Wattis, Discrete breathers in a two-dimensional Fermi-Pasta-Ulam lattice, J. Phys. A: Math. Gen. **39**, 4955 (2006).
[44] N. I. Aleksandrova, The propagation of transient waves in two-dimensional square lattices, Int. J. Solids Struct. **234-235**, 111194 (2022).
[45] K. A. Krylova, E. A. Korznikova, A. S. Semenov, D. V. Bachurin, and S. V. Dmitriev, Linking tracks in mica crystals with phase transitions in a bistable lattice, Eur. Phys. J. B **93**, 23 (2020).
[46] F. M. Russell and J. C. Eilbeck, Evidence for moving breathers in a layered crystal insulator at 300 K, EPL **78**, 10004 (2007).
[47] J. Bajars, J. C. Eilbeck, and B. Leimkuhler, Nonlinear propagating localized modes in a 2D hexagonal crystal lattice, Phys. D (Amsterdam, Neth.) **301-302**, 8 (2015).
[48] J. Bajars, J. C. Eilbeck, and B. Leimkuhler, in *Quodons in Mica*, Springer Series in Materials Science Vol. 221, edited by J. Archilla, N. Jimenez, V. Sanchez-Morcillo, and L. Garcia-Raffi (Springer, Cham, 2015), p. 35.
[49] J. Bajārs, J. C. Eilbeck, and B. Leimkuhler, Two-dimensional mobile breather scattering in a hexagonal crystal lattice, Phys. Rev. E **103**, 022212 (2021).
[50] Y. Sun, Z. Zhuo, X. Wu, and J. Yang, Room-temperature ferromagnetism in two-dimensional $Fe_2Si$ nanosheet with enhanced spin-polarization ratio, Nano Lett. **17**, 2771 (2017).
[51] Y. Peng, W. Li, F. Wang, T. Still, A. G. Yodh, and Y. Han, Diffusive and martensitic nucleation kinetics in solid-solid transitions of colloidal crystals, Nat. Commun. **8**, 14978 (2017).
[52] V. A. Kuzkin, A. M. Krivtsov, E. A. Podolskaya, and M. L. Kachanov, Lattice with vacancies: Elastic fields and effective properties in frameworks of discrete and continuum models, Philos. Mag. **96**, 1538 (2016).
[53] C. Chong, Y. Wang, D. Marechal, E. G. Charalampidis, M. Moleron, A. J. Martinez, M. A. Porter, P. G. Kevrekidis, and C. Daraio, Nonlinear localized modes in two-dimensional hexagonally-packed magnetic lattices, New J. Phys. **23**, 043008 (2021).
[54] Y. Dai, H. Yu, Z. Zhu, Y. Wang, and L. Huang, Discrete breathers and energy localization in a nonlinear honeycomb lattice, Phys. Rev. E **104**, 064201 (2021).

[55] C. Fang, N. Wang, and X. Shen, Tunable band gap in distorted square lattice's phonon spectrum, Results Phys. **29**, 104697 (2021).

[56] S. M. Bak and G. M. Kovtonyuk, Existence of periodic traveling waves in Fermi-Pasta-Ulam-type systems, J. Math. Sci. **260**, 619 (2022).

[57] Y. Doi and A. Nakatani, Intrinsic localized mode as in-plane vibration in two-dimensional Fermi-Pasta-Ulam lattices, Nonlinear Theory Appl., IEICE **3**, 67 (2012).

[58] W. Feng, B. Tang, L. Wu, P. Kong, C. Yang, L. Wang, and K. Deng, Nonlinear localized excitations in a topological ferromagnetic honeycomb lattice, J. Magn. Magn. Mater. **536**, 168089 (2021).

[59] N. S. Bakhvalov, *Numerical Methods: Analysis, Algebra, Ordinary Differential Equations* (MIR, Moscow, 1977).